34th IAHR World Congress – Balance and Uncertainty
33rd Hydrology & Water Resources Symposium
10th Hydraulics Conference

26 June – 1 July 2011, Brisbane, Australia

Numerical investigation of flow and sediment transport around a circular bridge pier

S. Abdelaziz[1], M.D. Bui[1], and P. Rutschmann[1]

[1]Institute of Hydraulic and Water Resources Engineering, Technische Universität München, Munich, Germany

E-mail: shokry@bv.tu-muenchen.de

Abstract: *A computation module for sediment transport in open channels was developed and incorporated into the commercial code FLOW-3D. In the module, the bed-load transport is simulated with a non-equilibrium model. Effects of bed slop and material sliding are also taken into account. The bed deformation is obtained from an overall mass-balance equation for sediment transport. This paper presents the results of a model application to compute the temporal variation of flow and scour around a circular bridge pier. The experimental investigation has been carried out by Unger and Hager (2006). The predictions are compared with measurements of flow and bed deformation, for which the results show generally good agreement.*

Keywords: *Scour, Sediment Transport, Numerical Modelling, Bridge Pier*

1. INTRODUCTION

The three-dimensional flow field around a pier is extremely complex due to separation and generation of multiple vortices. The complexity of the flow field is further magnified due to the dynamic interaction between the flow and the moveable boundary during the development of a scour hole (see Raudkivi, 1986; Esmaeili et al., 2009). Accurate prediction of scour patterns around bridge piers strongly depend on resolving the flow structure and the mechanism of sediment movement in and out of the scour hole (Mendoza-Cabrales, 1993). Turbulence and the induced secondary flow field around the bridge element have been studied intensively in the last years both experimentally (e.g., Unger and Hager, 2007; Muzzammil and Gangadhariah, 2003; Melville and Raudkivi 1977) and numerically (e.g., Dou, 1997; Nagata et al., 2002; Esmaeili et al., 2009).

FLOW-3D is a commercial package developed by Flow Science Inc at Los Alamos Scientific Lab (Flow Science Inc., 2008). The software uses several special features for numerical solution of the Navier-Stokes equations for free surface flows (VOF-method) and meshing of complicated geometries (FAVOR method). The sediment scour model treats sediment as two concentration fields (Brethour, 2003): the suspended sediment and the packed sediment. The suspended sediment advects and drifts with the fluid due to the influence of the local pressure gradient. Suspended sediment originates from inflow boundaries or from erosion of packed sediment. The packed sediment, which does not advect, represents sediment that is bound by neighboring sediment particles. From the physical point of view, the assumption of the two concentration fields seems to be valid to model fine sediment bed materials. However, for coarse bed materials, it could be incorrect and we could not get acceptable results in this case. In a previous study by the authors (Abdelaziz et. al., 2010) , a reasonable agreement between the predicted results and measurements of bed profile, maximum scour depth and maximum deposition after few minutes of simulation time were obtained. However, calculation results for the later stages of scour development were significantly under estimated. While the deposition rate increases with time in the experiment, the predicted deposition rate starts to decrease after few minutes of simulation. The results showed an agreement with Smith (2007) results.

A computation module for non-cohesive sediment transport in open channels was developed at the Institute of Hydraulic and Water Resources Engineering, Technische Universität München and incorporated into FLOW-3D. In this module, suspended transport is simulated through the general convection-diffusion equation with an empirical settling velocity term and the exchange of suspended sediment and bed-load at the lower boundary of the suspended sediment layer. Bed-load transport is simulated with a non-equilibrium model and the bed deformation is obtained from an overall mass-balance equation. In the module, effects of bed slope and bed material sliding on the sediment transport are also taken into account. This paper presents the validation of the developed module for

bed-load transport with data from laboratory measurements. Further, the sensitivity of the model parameters is investigated.

2. GOVERNING EQUATIONS

2.1. Hydrodynamic module

The hydrodynamic module is based on the solution of the three-dimensional Navier-Stokes equations and the continuity equation. The continuity equation and the model formulation of the Navier- Stokes equations for incompressible flows used in FLOW-3D are as follows (Flow Science Inc., 2008):

$$\frac{\partial}{\partial X_i} U_i A_i = 0$$
(1)

$$\frac{\partial U_i}{\partial t} + \frac{1}{V_f}\left(U_j A_j \frac{\partial u_i}{\partial X_j}\right) = -\frac{1}{\rho}\frac{\partial P}{\partial X_i} + G_i + f_i$$
(2)

where:

$$\rho V_f f_i = \tau_{b,i} - \left[\frac{\partial}{\partial X_j}(A_j S_{ij})\right]; S_{ii} = -2\mu_{tot}\left[\frac{\partial U_i}{\partial X_i}\right]; S_{ij} = -\mu_{tot}\left[\frac{\partial U_i}{\partial X_j} + \frac{\partial U_j}{\partial X_i}\right].$$
(3)

where U_i=mean velocity; P=pressure; A_i=fractional open area open to flow in the i direction; V_f =fractional volume open to flow; G_i represents the body accelerations; f_i represents the viscous accelerations; S_{ij}=strain rate tensor; τ_b, i=wall shear stress; ρ=density of water; μ_{tot}=total dynamic viscosity, which includes the effects of turbulence ($\mu_{tot}=\mu+\mu_T$); μ=dynamic viscosity; and μ_T=eddy viscosity.

The wall boundary conditions are evaluated differently based on the chosen turbulence closure scheme. Transport turbulence closure schemes (e.g., k-ε model) use a law of the wall formulation. The combined smooth and rough logarithmic law of the wall equation is iterated in order to solve for the shear velocity u* (Flow Science Inc., 2008; Smith and Foster., 2005):

$$u_o = u_*\left[\frac{1}{\kappa}\ln\left(\frac{\rho u_* y_o}{\mu + \rho a u_* K_s}\right) + 5.0\right]$$
(4)

where κ=von Karman constant; a is a constant, which is equal to 0.247 for k-ε and RNG models, or 0.246 otherwise; K_s is the roughness; and y_0=distance from the solid wall to the location of tangential velocity, u_0. The denominator of Eq. (4) represents an effective viscosity due to the effect of the rough boundary ($\mu_{eff} = \mu+\rho a u*ks$). If the cell is within the laminar sublayer ($\rho u*y_0 /\mu\le5.0$), the solution for the shear velocity is defined with:

$$u_* = \sqrt{\frac{\mu . u_o}{\rho y_o}}$$
(5)

For laminar flows and non-transport turbulence closure schemes (e.g., LES models), the wall shear stress $\tau_{b,i}$ is defined with

$$\tau_{b,i} = \frac{(\mu + \rho a u_o k_s) u_o}{y_o}$$
(6)

The model has several different turbulence closure schemes, including one-equation turbulent energy (k), two-equation (k-ε), renormalization-group (RNG), and large eddy simulation (LES) closure schemes. The k-ε closure scheme will be considered as the transport closure scheme in this paper. The standard k-ε model (Wilcox 2000) approximates the eddy viscosity with

$$\mu_T = \frac{\rho C_\mu k^2}{\varepsilon}$$
(7)

The closure equations for the turbulent kinetic energy, k, and the dissipation rate, ε, are given by:

$$\frac{\partial k}{\partial t} + \frac{1}{V_f}U_i A_{xi}\frac{\partial k}{\partial X_i} = C_{sp}\frac{\mu}{\rho V_f}\left\{2A_{xi}\left(\frac{\partial U_i}{\partial X_i}\right)^2 + \left(\frac{\partial U_i}{\partial X_j} + \frac{\partial U_j}{\partial X_i}\right)\left(A_{xj}\frac{\partial U_i}{\partial X_j} + A_{xi}\frac{\partial U_j}{\partial X_i}\right)\right\} - \frac{1}{V_f}\frac{\partial}{\partial X_j}\left[\frac{A_{xi}}{\rho}\left(\mu + \frac{\mu_T}{\sigma_k}\right)\frac{\partial k}{\partial X_j}\right]$$
(8)

where C_{sp} is the shear production coefficient.

$$\frac{\partial \varepsilon}{\partial t} + \frac{1}{V_f} U_i A_{xi} \frac{\partial \varepsilon}{\partial x_i} = C_{\varepsilon 1} \frac{\varepsilon}{k} \left(C_{sp} \frac{\mu}{\rho V_f} \left(2 A_{xi} \left(\frac{\partial U_i}{\partial X_i} \right)^2 + \left(\frac{\partial U_i}{\partial X_j} + \frac{\partial U_j}{\partial X_i} \right) \left(A_{xj} \frac{\partial U_i}{\partial X_j} + A_{xi} \frac{\partial U_j}{\partial X_i} \right) \right) \right) - \frac{1}{V_f} \frac{\partial}{\partial X_j} \left[\frac{A_{xi}}{\rho} \left(\mu + \frac{\mu_T}{\sigma_k} \right) \frac{\partial k}{\partial X_j} \right] - C_{\varepsilon 2} \frac{\varepsilon^2}{k}$$

(9)

The closure coefficients and auxiliary relations in case of K-ε are: ($C_{\varepsilon 1}$= 1.44, $C_{\varepsilon 2}$ = 1.92, C_μ = 0.09, σ_k = 1.0, σ_ε = 1.3), while in RNG model: ($C_{\varepsilon 1}$= 1.42, $C_{\varepsilon 2}$ is a is a function of the shear rate, C_μ = 0.085, σ_k = 0.72, σ_ε = 0.72)

The Reynolds-stress tensor, τ_{ij}, and the mean strain-rate tensor, e_{ij}, are defined with

$$\tau_{ij} = 2 \frac{\mu_T}{\rho} e_{ij} - \frac{2}{3} k \delta_{ij}$$

(10)

$$e_{ij} = \frac{1}{2} \left(\frac{\partial U_i}{\partial Xj} + \frac{\partial U_j}{\partial X_i} \right)$$

(11)

The boundary conditions for k and ε are computed using the logarithmic law of the wall formulation and are defined with

$$k = \frac{u_*^2}{\sqrt{C_\mu}} ; \varepsilon = \frac{u_*^3}{\kappa y_o}$$

(12)

FLOW-3D handles free surfaces using a method known as the Volume of Fluid (VOF) technique pioneered by Hirt and Nichols (1981). This technique consists of three components: a method for finding the free surface, an algorithm for tracking the free surface as a sharp interface moving through the computational mesh and a process for applying boundary conditions to the surface. The method makes use of the simple principle of assigning a single variable F (fluid fraction) to each cell that has a value of 1.0 if the cell is occupied by fluid and a value of 0.0 if the cell is completely empty. Therefore, if the cell has a value of F between 0.0 and 1.0 then the cell contains a free surface. In addition, the normal to the surface can be calculated from the direction in which F changes most rapidly applying boundary conditions to the surface.

$$\frac{\partial F}{\partial t} + \frac{1}{V_f} \left[A_x u \frac{\partial F}{\partial X} + A_y v \frac{\partial F}{\partial Y} + A_z w \frac{\partial F}{\partial Z} \right] = 0$$

(13)

FLOW-3D permits the modeling of complicated geometries by allowing the partial blockage of each cell in a regular mesh. The partial blockage of mesh cells is represented by associating a single volume fraction (V_f) and three area fractions (A_x, A_y, and A_z) with each computational mesh cell. The volume fraction is the fraction of the cell volume which may be occupied by fluid. It is, therefore, one minus the fraction of the cell volume which is occupied by solid material. The area fractions are defined as the fraction of the area of each mesh cell face through which fluid may flow. Those associated with a particular cell are the faces between it and the next higher cell in the x, y, and z directions. The other three faces of a particular cell have area fractions that are associated with the next lower cell in each direction (Sicilian, 1990).

2.2. Bed-load transport module

The bed level change z_b is calculated from the overall mass balance equation for bed load sediment.

$$(1 - p') \frac{\partial Z_b}{\partial t} + \frac{\partial Q_{bs}}{\partial s} + \frac{\partial Q_{bn}}{\partial n} = 0$$

(14)

where p' is porosity of the bed material; Q_{bs}, Q_{bn} are bed-load flux in main-flow direction s and cross-flow direction n. They are calculated from the non-equilibrium bed-load equation:

$$\frac{\partial (Q_b \alpha_{bs})}{\partial s} + \frac{\partial (Q_b \alpha_{bn})}{\partial n} = -\frac{1}{L_s} (Q_b - Q_e)$$

(15)

where α_{bs}, α_{bn} are direction cosines determining the components of the bed-load transport in the s and n directions, respectively. This is the mass balance equation for bed-load sediment transport in which all non-equilibrium effects are expressed through the model on the right hand side, assuming the effects to be proportional to the difference between non-equilibrium bed-load Q_b and equilibrium bed-load Q_e and related to the non-equilibrium adaptation length L_s. Both Q_e and L_s are determined from empirical formulae (Bui and Rutschmann, 2010).

In the literature many formulas for equilibrium bed-load transport can be found. Most of them relate bed load transport rate with effective shear stress. In this study, the well-known two formulae developed by Van Rijn (1984) and Mayer Peter Müller (1948) are applied. According to Van Rijn (1984) the equilibrium bed load can be calculated as:

$$Q_e = 0.053(\frac{\rho_s - \rho}{\rho} g)^{0.5} \frac{d_{50}^{1.5} T^{2.1}}{D_*^{0.3}} \quad ; \quad D_* = d_{50} \left[\frac{(\rho_s - \rho)g}{\rho v^2} \right]^{1/3} ; T = \frac{(U_*')^2 - (U_{*cr})^2}{(U_{*cr})^2} \tag{16}$$

where U_*' is the effective bed shear velocity corresponding to the grain, and U_{*cr} is the critical bed shear velocity for incipient motion given by the Shields diagram. On the other hand, the Peter Müller (1948) formula is:

$$Q_e^* = 8 \left[\left(\frac{C}{C_{90}} \right)^{3/2} \theta - \theta_{cr} \right]^{3/2} \left(\frac{\rho_s}{\rho} g d_{50}^3 \right)^{-1/2} ; \theta_{cr} = 0.047 \tag{17}$$

in which C = Chézy friction coefficient; C_{90} = grain related Chézy value; θ = fractional Shields parameter; $θ_{cr}$ = critical Shields value.

Generally, the non-equilibrium adaptation length L_s is related to the dimensions of sediment movements, bed forms, and channel geometry. The non-equilibrium adaptation length for bed load may take the value of the average saltation step length of particles or the length of ripples. Phillips and Sutherland (1989) proposed the following equation for the average saltation step length:

$$L_s = \alpha_p (\theta - \theta_{cr}) d_{50} \tag{18}$$

where $α_p$ is constant. The average saltation step length can also be calculated from an empirical formula of Van Rijn (1987):

$$L_s = 3 d_{50} D_*^{0.6} T^{0.9} \tag{19}$$

Because the bed load transport formula was derived for nearly horizontal bed, it cannot approximate the effect of bed slope. In the present study influence of bed slope on the bed load transport is taken into account by correcting the critical bed shear stress of Shields for slope effect both in longitudinal and transverse directions as suggested by Dey (2001, 2003)

$$\tau_{cr\_eff} = 0.954 \tau_{cr} (1 + \frac{\theta_s}{\Phi})^{0.745} (1 + \frac{\theta_n}{\Phi})^{0.372} \tag{20}$$

where $τ_{cr}$ is the critical shear stress; $θ_n$, $θ_s$ are longitudinal and transverse slope angles; Φ is angle of repose. Before the new flow iterations were commenced the bed was checked for location where the bed slope was larger than the angle of repose. At such locations the sediment will, due to gravity, move in the direction of the steepest slope until the slope is lower than the angle of repose. A description of such land slide has been implemented in the model. This sand-slide effect was also previously taken into account in the work of Roulund (2004) and Olsen et al. (1998) and can well be observed in physical model studies.

In the computer code FLOW-3D, the flow and sediment transport modules communicate through a quasi-steady morphodynamic time-stepping mechanism: during the flow computation the bed level is assumed constant and during the computation of the bed level the flow and sediment transport quantities are assumed invariant to the bed level changes. This procedure can be described as follows: The bed shear stress calculated from the flow module at each time step is used to calculate the equilibrium bed-load and related parameters. Non-equilibrium bed-load is applied for calculation of bed change. The effects of the bed change on flow field are taken into account by updating the open volume fraction and the flow field as well as the pressure near the bed as follows:

(i)   The change in volume of fluid is equal to the change in bed elevation at this cell.
(ii)   If the updated volume of fluid is greater than one, this cell will be totally filled with fluid (V_f =1.0) and the remaining volume of fluid will be added to the lower cell.
(iii)   If the updated volume of fluid is less than zero, this cell will be fully blocked (V_f =0.0) and the upper cell will become the boundary cell.

The fraction areas in x-direction (A_x), y-direction (A_y), and z-direction (A_z) are defined as the average of the volume of fluid of the attached cells.

The vertical velocity at the first mesh point from bed is set to be the same as the bed elevation change velocity. This adjustment is particularly important in the early stages of scour.

3. CALCULATION RESULTS AND DISCUSSIONS

Experimental investigations of temporal flow evolution of sediment embedded circular bridge piers

have been carried out by Unger (2006). Measured data were used to validate our numerical model. In this experiment, the hydraulic model test was conducted in a scouring channel of VAW-ETHZ, with a maximum discharge of Q=130 l/s and a maximum water depth of 0.4 m. The rectangular channel had a width of 1 m and a length of 13 m with working section of 5 m. A semicircular plexiglass pier was placed at the glassed channel sidewall, to allow for optical flow visualization. Run D6 of the experiment was chosen as a typical run to be simulated. The bed material is sand with d_{50}=1.14 mm. The flow condition for this run is as follows: The inlet velocity is 0.391m/s and the flow is 0.025 m^3/s. The downstream water depth is controlled to be 0.064 m. The bridge pier diameter was 0.26 m. The numerical model was set up according to the experimental conditions RUN D6. Morphological calculations started with still water and horizontal bed.

A choice of the computational mesh was based on the quality of the input data, the computer capacity and the accuracy of the numerical solution. A series of test for different mesh sizes have been done. A uniform mesh of 1,330,000 elements with 1.0 cm grid size in X and direction and 0.5 cm in Z direction was selected.
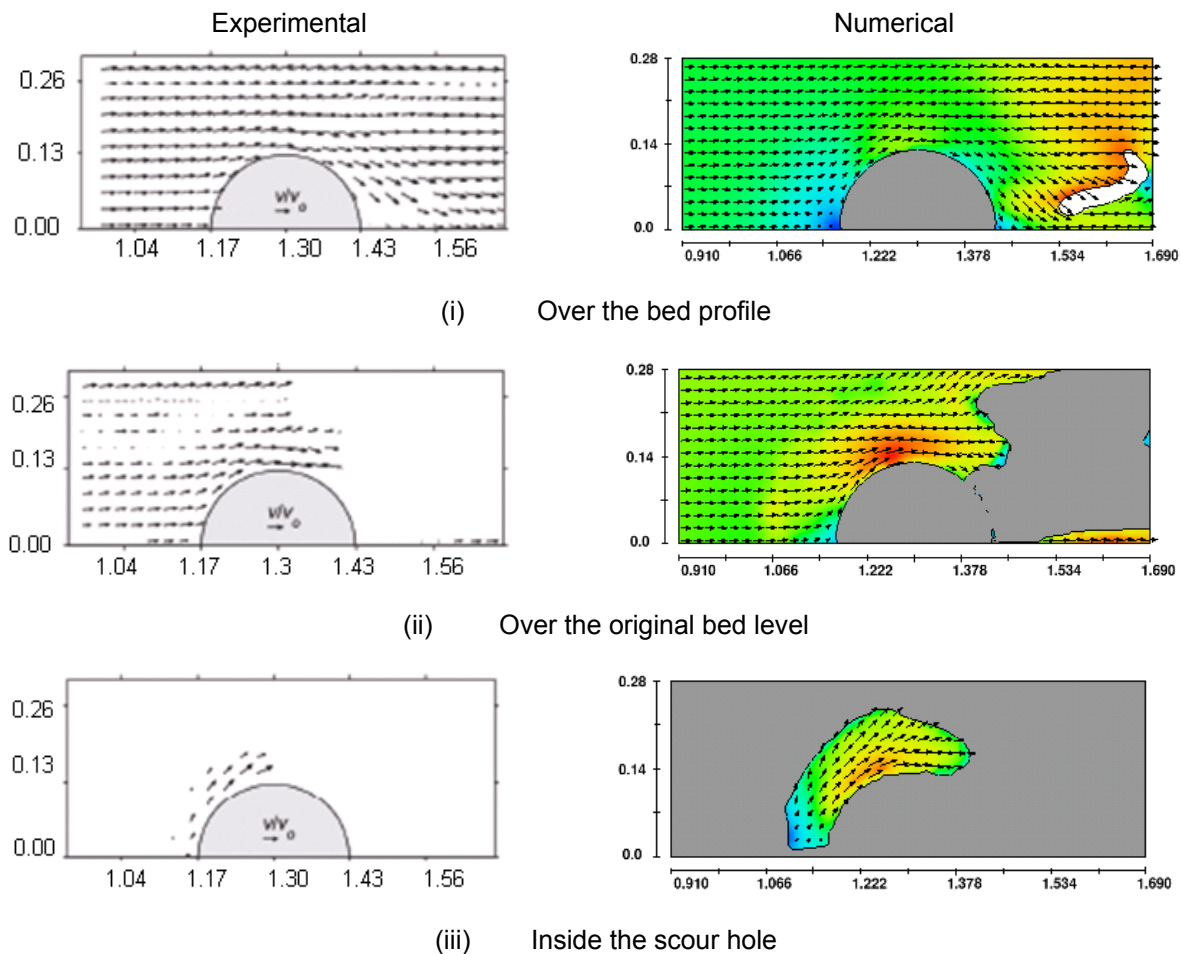

(i)   Over the bed profile

(ii)   Over the original bed level

(iii)   Inside the scour hole

Figure 2: Flow velocity and scour topography for RUN D6 in various planes

To adjust the hydraulic parameters of the model, the numerical model ran first for hydraulic calculation with RNG turbulence model with the bed profile after 3 minutes. Figure 1 refers to the analogous flow fields in three horizontal planes, namely (1) over the bed profile, (2) at the original bed surface and (3) inside the scour hole as mentioned by Unger and Hager (2006). Over the bed profile, the flow field upstream from the pier is relatively uniform, as reflected by the parallel and constantly spaced streamlines. Closer to the pier (distance of 0.13 m from pier), the flow is deflected in the transverse channel direction y and accelerated, with the maximum velocity at an angle of 75°, resulting there in sediment entrainment. Simultaneously, the pressure along the pier decreases to its minimum at 75°. Beyond this region at an angle between 90° and 120°, the flow separates from the pier due to the well-known pressure increase (Schlichting and Gersten 1997). The same situation can be seen for

both the experiment and simulation model while in the numerical model, the separation zone is smaller than in the experiment.

The flow of the plane at the original bed level is more complex than the previous plane. Whereas upstream of the pier in a distance larger than 0.13 m from the pier, only minor differences are visible compared to the previous plane. The stream lines are still parallel. Closer to the pier, the flow deflect in the transverse direction with maximum velocity at 75°. The instantaneous scour circumference generates a separation line.

Consider now the flow field in the horizontal plane inside the scour hole, a source flow develops at the pier front, due to the down-flow. The source flow is deflected in the transverse channel direction along the pier perimeter. This is in agreement with the vertical flow fields shown in Figure 2, containing no recirculation in the scour hole. A good agreement can be seen between the numerical model and experimental results.

A characteristic example of the flow field close to the channel symmetry axis at y = 30 mm is shown in Figure 3, the streamlines in the approach flow region are nearly parallel such that the flow is not affected by the presence of the pier and the vertical velocity profiles have a standard logarithmic distribution. It was demonstrated that the effect of the pier on the upstream flow field extends to approximately a distance of $x = -(h_o D^2)^{1/3}$ measured from the leading pier front, where h_o is the approach flow depth and D is the diameter of the pier (Unger, 2006). Closer to the pier, the scour has migrated from the pier side to the symmetry plane, without an appreciable change of the flow in the approach flow region. From the boundary of the scour hole a vertical flow deflection toward the instantaneous sediment surface is observed. Furthermore, the down and up-flows, the surface recirculation and the stagnation point have established. The down-flow is deflected in the transverse channel direction along the scour surface.
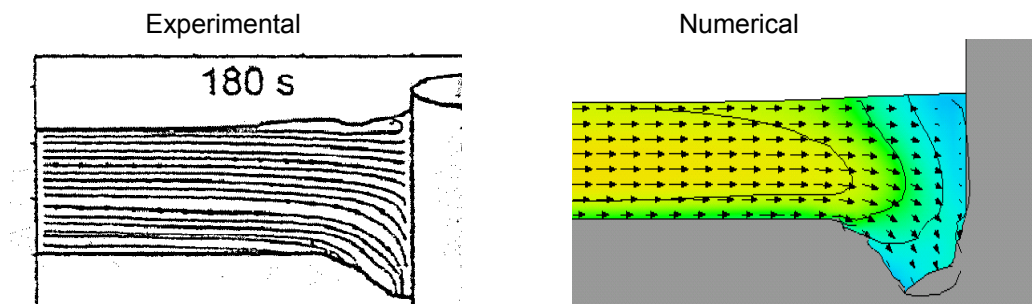
Experimental   Numerical

Figure 3: Stream line and velocity at time 3 minutes for RUN D6

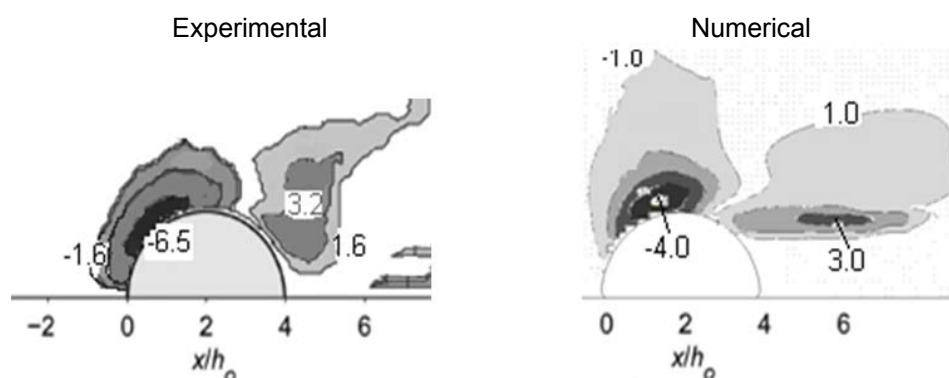Experimental   Numerical

Figure 4: scour topography for RUN D6 at time 60 sec (contours in cm)

It can be seen in Figure 3, the model can simulate well the flow characteristic around the pier with a minor difference from experimental data.

The contours around the pier obtained at the end of 1 min of test duration are shown in Figure 4. It was observed that the scour starts from an angle about 75°. While the predicted place of maximum scour and deposition agrees well with the measurement, the results of numerical model simulations of local scour for the pier are underestimated. No scour or deposition can be seen beside the wall. It indicates that the computed scouring pattern is reasonable in qualitatively good agreement with those from the experiments conducted by Unger (2006). In order to get quantitatively good results, the model needs further developments. Among others, including suspended sediment transport in the model may also enhance the simulated results.

4. CONCLUSION

A 3D sediment transport model was developed and integrated into FLOW-3D. In the module, the bed-load transport is simulated with a non-equilibrium model. Effects of bed slope and material sliding are also taken into account. The bed deformation is obtained from an overall mass-balance equation for sediment transport. Further, the sensitivity of the simulated results is investigated by applying the model to an experiment for temporal flow evolution of sediment embedded circular bridge piers. The results show that the model could predict accurately the flow characteristic around the bridge pier. Further, the scour model showed a good qualitative result compared to the model scour conducted in the laboratory. The scour hole starts at angle 75°. The position of the scour and deposition match the experiment. However, further works are needed to enhance the model and complete numerical simulation of the experiment.

5. NOTATION

The following symbols are used in this paper:

A_i = fractional area open to flow in i direction;
a = model constant;
C = Chézy friction coefficient;
C_{90} = grain related Chézy value;
d_{50} = median grain size;
D_* = non dimension sediment grain size;
F = fluid fraction;
G_i = body accelerations;
k = turbulent kinetic energy;
K_s = wall roughness;
L_s = non-equilibrium adaptation length;
n_s = unit vector normal to bed;
P = pressure;
p' = porosity of the bed material;
Q_b = non-equilibrium bed-load;
Q_e = equilibrium bed-load;
S_{ij} = strain rate tensor;
U_i = mean velocity;
U_*' = effective bed shear velocity corresponding to the grain;
U_{*cr} = critical bed shear velocity for incipient motion given by the Shields diagram;
V_f = fractional volume open to flow;
$\tau_{b,i}$ = wall shear stress;
τ_{cr} = critical shear stress;
τ_{cr_eff} = effective critical shear stress;
α_{bs}, α_{bn} = direction components of the bed-load transport in the *s* and *n* direction;
θ = fractional Shields parameter;
θ_n, θ_s = longitudinal and transverse slope angle;
θ_{cr} = critical Shields value;
Φ = angle of repose;

ρ = water density;
ρ_s = sediment density;
μ = dynamic viscosity;
μ_τ = eddy viscosity;
κ = Von Karman constant;
ε = turbulent dissipation rate

6. REFERENCES

Abdelaziz, S., Bui, M.D., and Rutschmann, P. (2010), *Numerical simulation of scour development due to submerged horizontal jet*, 5th River Flow, International Conference on Fluvial Hydraulics.

Brethour, J. (2003), *Modeling Sediment Scour*, Flow Science, Inc. Report FSI-03-TN62

Bui, M.D., and Rutschmann, P. (2006), *Numerical modelling of non-equilibrium graded sediment transport in a curved open channel*, Computers & Geosciences, Vol. 36, 792-800.

Dey, S. (2001), *Experimental Studies on Incipient Motion of Sediment Particles on Gerneralized Sloping Fluvial Beds*, J. Sediment Research, Vol. 16 (3), 391-398.

Dey, S. (2003), *Threshold of sediment motion on combined transverse and longitudinal sloping beds*, J. Hydraulic of Research, Vol. 41(4), 405–415.

Dou, X. (1997), *Numerical Simulation of Three-Dimensional Flow Field and Local Scour at Bridge Crossings*, Ph.D. Dissertation, University of Mississippi, Oxford, MS, U.S.A.

Esmaeili, A. A. Dehghani, A. R. Zahiri and K. Suzuki. (2009), *3D numerical simulation of scouring around bridge piers (Case study: bridge 524 crosses the Tanana river)*, World Academy of Science, Engineering and Technology 58.

Flow Science, Inc. (2008), *FLOW-3D User's Manual*, Flow Science, Inc.

Hirt, C.W. and Nichols, B.D. (1981), *Volume of Fluid (VOF) Method for the Dynamics of Free Boundaries*, J. Computational Physics, Vol. 39, 201-225.

Mendoza-Cabrales, C. (1993), *Computation of flow past a pier mounted on a flat plate*, Proc. ASCE Water Resources Engineering Conf., San Francisco, 1993, 899-904.

Melville, B. W. and Raudkivi, A. J. (1977), *Flow characteristics in local scour at bridge piers*, Journal of Hydraulic Research, 15:373–380.

Meyer-Peter, E., and Müller, R. (1948), *Formulas for bed-load transport*, Proc., 2nd Meeting, IAHR, Stockholm, Sweden, 39-64.

Muzzammil, M. and Gangadhariah, T. (2003), *The mean characteristics of horseshoe vortex at a cylindrical pier*, J. Hydraulic Research Vol. 41(3), 285–297.

Nagata, N., Hosoda, T., Nakato, T. and Muramoto, Y. (2002), *3D numerical simulation of flow and local scour around a cylindrical pier*, J. Hydrosci. Hydraul. Eng., Vol.20 (1), 113-125.

Olsen, N. R. B., and Kjellesvig, H. M. (1998), *Three- dimensional numerical flow modeling for estimation of maximum local scour*, J. of Hydraulic Res., Vol. 36(4), 579-590.

Phillips, B. C., and Sutherland, A. J. (1989), *Spatial lag effects in bed load sediment transport*, J. of Hydraulic Res., Vol. 27(1), 115–133.

Raudkivi, A. J. (1986), *Functional trends of scour at bridge piers*, J. Hydr. Eng., Vol.112 (1), 1–13.

Roulund, A. (2000), *Three- dimensional numerical flow modeling of flow around a bottom mounted pile and its application to scour*, PhD thesis, Department of Hydrodynamics and Water Resources, TU Denmark, Series Paper No. 74.

Sicilian, J. (1990), *A "Favor" based moving obstacle treatment for FLOW-3D*, Flow Science, Inc. Internal publication (FSI-90-00-TN24).

Schlichting H, Gersten K. (1997), *Grenzschicht-Theorie*, Springer, Berlin Heidelberg New York.

Smith, H. (2007), *Flow and sediment dynamics around three-dimensional structures in coastal environments*, Ph.D. thesis, The Ohio State University.

Smith, H., and Foster, D. (2005), *Modeling of Flow Around a Cylinder Over a Scoured Bed*, J. of waterway, port, coastal, and ocean engineering, 10.1061/(ASCE)0733-950X(2005)131:1(14).

Unger, J., and Hager, W. H. (2007), *Down-flow and horseshoe vortex characteristics of sediment embedded bridge piers*, J. Exp. Fluids, 42, 1–19.

Unger, J. (2006), *Strömungscharakteristika um kreiszylindrische Brückenpfeiler - Anwendung von Particle Image Velocimetry in der Kolkhydraulik*, PhD thesis 16557.ETH, Zurich.

Unger, J., and Hager, W. H. (2006), *Temporal flow evolution of sediment embedded circular bridge piers*, River Flow 2006, 1:729–739, Taylor & Francis Group, London.

Van Rijn, L.C. (1984), *Sediment transport, part I: bed load transport*, J. Hydraulic Engineering, Vol. 110(10), 1431-1456.

Van Rijn, L.C. (1987), *Mathematical modeling of morphological processes in the case of suspended sediment transport*, PhD thesis, Faculty of civil engineering, Delft University of technology.

Wilcox, D.C. (2000), *Turbulence Modelling for CFD*, Second Edition, DCW Industries Inc., California.